Ground Structure Approaches for the Evolutionary Optimization of Aircraft Wing Structures

Teemu J. Ikonen* and András Sóbester†

University of Southampton, Southampton, Hampshire, SO16 7QF, United Kingdom

Aircraft wings have seen very few changes in the topological arrangement of the internal structures during the past decades. However, the traditional topology consisting of longitudinal spars and transverse ribs has not been conclusively shown to be the optimal. The purpose of this study is to develop a tool to explore the space of alternative internal structure topologies. We consider a pair of two-step optimization methods. First, a large set of potential structural members, i.e. a ground structure, is built inside the outer mold line of the wing. Second, an evolutionary optimization method is applied to search for the optimal subset of structural members. Two methods are used: a genetic algorithm (GA) and an evolutionary structural optimization (ESO) heuristic. The objective in both cases is to minimize the structural mass of the wing subject to stress and buckling constraints, which are evaluated by automated finite element analysis. The methods are applied to the structural design of the 3D printed wing of a small unmanned aerial vehicle (sUAV) and benchmarked against manually designed internal structures.

I. Introduction

A. Motivation

The Wright brothers constructed their first aircraft wings using wood and fabric, with a structural arrangement consisting of longitudinal spars and transverse ribs. During World War I aircraft engineers introduced cantilever wings free of external struts or wires that cause unnecessary drag. The skin material was changed from fabric to wooden veneer, which enabled so called *stressed skin* designs leading to a reduction in wing mass.[1] For the first time spars, ribs, and stressed skins formed the load carrying wing box structure. Further, longitudinal stringers were attached to the skin panels of the wing box to prevent buckling. This structural arrangement is still widely used in aircraft design, regardless of the growing range of new materials. However, it is questionable if the arrangement of longitudinal spars and stringers, and transverse ribs is optimal in terms of the structural mass of the wing.

An excellent test platform for new internal structure topologies is afforded by small unmanned aerial vehicles (sUAVs). In comparison to larger aircraft, sUAVs have a very rapid design and manufacturing process, in which new technologies can be conveniently tested. Recently, 3D printing (additive manufacturing) has enabled even quicker manufacturing of sUAV components with almost no constraints on shape and topology. Using 3D printing, a sUAV wing can be manufactured overnight as a single part, where the internal structure and the skin are parts of the same component.

We were motivated to write this paper by two related objectives. The first is to explore alternative arrangements for wing internal structures in the specific case of a 3D printed sUAV wing. The second is to benchmark a genetic algorithm and an evolutionary structural optimization (ESO) heuristic against manually designed internal structures.

*Graduate Research Student, Computational Engineering and Design, Faculty of Engineering and the Environment, AIAA Student Member.

†Associate Professor, Computational Engineering and Design, Faculty of Engineering and the Environment, AIAA Senior Member.

B. Topology optimization in aircraft wing design

The first conceptual step in populating the inside of a given OML with a sensible load-bearing structure is to determine the topology - or layout - of the internal structure. The greatest challenge here is establishing the design space. In standard, continuous optimization problems this is simply a matter of defining the ranges of the design variables, but the space of topologies has no conventional design variables and thus no ranges either, as defined in the conventional sense. Ideally, the best design would be obtained by picking the best combination of internal members from the *structural universe*, which is an infinite collection of all permissible structural members that a design may contain. In reality this is not possible because an infinite number of objective function evaluations would be needed. Instead, the members may be picked from a *ground structure* that is a finite, but large, subset of the structural universe. The optimization problem is then defined as finding the subset of the ground structure that has the lowest mass, but does not violate any constraints. See Refs. 2–5 for examples of this approach.

Another approach to establishing the design space is to distribute homogeneous material inside the OML and discretize the material into finite elements, a method first presented by Bendsøe and Kikuchi[6] and referred as the *homogenization method*. Each element is then assigned a design variable describing its presence in the design. The design variable may be a binary value describing strict 0/1 material distribution or a scalar value allowing the density of the element to vary between 0 and 1. Such a parameterization method has been applied to aerospace applications in Refs. 7–10. A combination of the ground structure and homogenization methods was used in the study by Stanford and Dunning,[11] where the wing box is first seeded by a ground structure and then the homogenization method was applied on the members of the ground structure.

Stanford and Dunning[11] pointed out that the topology optimization studies on aircraft wings, such as by James and Martins[8] and Dunning et. al.,[9] do not yield spar-rib like structures if the homogenization method is used. They name two possible reasons for the observation. The first is that the physics of the model, its load cases or boundary conditions, or the constraints of the design variables were not implemented correctly in the formulation of the optimization procedure. The second is that nontraditional internal structures offer better performance than the traditional spar-rib structure. If the latter reason is true, their observation could trigger an important shift in the conservative field of aircraft structural design, where the traditional rib-spar topology has been used for decades.

Several papers have indicated that the addition of diagonally oriented structural members as part of the internal structure improves the total performance of the structure. This behavior is seen in the studies with curvilinear spars and ribs done by Locatelli et. al.[12] and Jutte et. al.[13] Eves et. al.[7] interpreted the results from the homogenization method to shell-type structures, and the final structure contains several diagonally orientated internal structures. In addition, the results from ground structure based topology optimization done by Lencus et. al.[5] contained many diagonal members.

The second step in the topology optimization procedure is to search for either the best combination of ground structure members or for the best distribution of homogeneous material. Several gradient based optimization methods have been implemented in topology optimization of aircraft wings: Solid Isotropic Material with Penalization (SIMP) (Refs. 7, 10, 11), Evolutionary Structural Optimization (ESO) (Ref. 5) and level set (Refs. 8, 9). The objective in all of these studies is to minimize the compliance of the structure subject to a volume constraint. Eves et. al.[7] minimized afterwards the mass of the structure subject to twist angle, von Mises stress and buckling constraints. However, at this point only the rib pitch and material thicknesses were used as design variables. Lencus et. al.[5] checked the structure afterwards against buckling and wing tip deflection constraints, but the constraints were not considered in the optimization process itself. Kelly et. al.[14] used ESO as a part of an automated design optimization method of the rear fuselage of a UAV.

An alternative approach is to search the entire design space through a global heuristic of some type, typically a population based method. The following population based optimization methods have been used in aerospace topology optimization: genetic algorithms (Refs. 4, 15), ant colony optimization (Ref. 3), and evolutionary strategies (Ref. 16). In fact, Refs. 3, 16 and 4 use also gradient based local searches along with the population based searches to improve the computational efficiency. The objective in Refs. 3, 4, 16 is to minimize the mass of the structure, whereas Kobayashi et. al.[15] determined a Pareto front between maximum stress and drag-over-lift-ratio of the wing.

Genetic algorithms store the genetic information in strings. In a classical one-dimensional encoding the string is a vector containing the elements with genetic information, whereas in the two-dimensional encoding

the elements are arranged in a matrix forms. The vast majority of GA-based optimization applications use one-dimensional encoding, while the use of two-dimensional (or higher) encodings is very rare. However, the physical design domains of many practical problems are two- or three-dimensional.[17] Bui and Moon[18] indicate that if such a problem is encoded into a one-dimensional string, a considerable amount of genetic information is lost. The benefit of multidimensional encoding is in the preservation of the *geographical linkage* between the bits. The geographical linkage means that two bits that are located close to each other in the string are more likely to survive together to the next generation than two randomly selected bits in the same string. The first application of two-dimensional encoding is due to Cohoon and Paris,[19] who applied two-dimensional encoding to the optimization problem of a VLSI circuit placement. Later, two-dimensional encodings have been used for example in scheduling optimization problems,[20,21] where the job schedule of multiple workers is optimized, and in graph partitioning problems.[22] Giger and Ermanni[23] used a so called graph-based parameterization in the evolutionary optimization of the topology, shape and size of a truss structure. The genetic information describing each candidate was stored in two-dimensional strings. Considering the two-dimensional nature of the ground structure arrangement inside a wing, genetic algorithm based optimizations could perhaps be improved by using two-dimensional strings. However, two-dimensional encoding has not yet been applied to the topology optimization of an aircraft wing (as far as were able to ascertain).

Aircraft wings are constructed of lightweight and slender structural members, which under a compressive load are prone to buckling. Eigenvalue based buckling analyses are included as an objective or a constraint function in several topology optimization papers, such as Refs. 24–26. However, these studies are conducted mainly on simple two-dimensional structures. Very few papers in the literature consider buckling as a constraint in aircraft wing topology optimization and evaluate it using an FE model of the whole wing structure. One rare exception is the work of Yang et. al.,[4] wherein the buckling constraint is included as a penalty function in a genetic algorithm (GA) based optimization procedure. Lencus et. al.[5] mention buckling as a constraint, but do not evaluate it during the optimization process. Instead, buckling constraints are checked after the optimization process.

C. Approach to the problem

The approach in this study is to generate a large set of structural members, i.e. a ground structure, inside the wing, and to search for the optimal combination of members that has the lowest mass but satisfies both the stress and buckling constraints. The constraints are analyzed using an FE model of the whole wing structure, which provides more accurate estimations for the constraints than empirical estimates or FE models involving only a section of the wing. The search is conducted using two alternative evolutionary optimization methods: a genetic algorithm (GA) and an evolutionary structural optimization heuristic (ESO). In the GA-based optimization both one- and two-dimensional strings are tested and a comparison is made. The constraints are included using a penalty function. The ESO-based optimization is also tested using a bi-directional (BESO) approach where members can be recovered.

II. Methods

The objective of the optimization framework is to minimize the structural mass of the wing, W_s, subject to stress and buckling constraints. The optimization problem is defined as

$$\begin{array}{rcl} \text{minimize} & W_s(x) & \\ \text{w.r.t} & x_i & i = 1, 2, \ldots, m \\ \text{subject to} & \sigma_i^{max} \leq \sigma^{limit} & i = 1, 2, \ldots, n. \\ & \lambda_1 \geq 1, & \end{array} \tag{1}$$

where x is a vector of m design variables, σ_i^{max} is the maximum von Mises stress in *material section* i (with a total of n sections), σ^{limit} is the maximum allowed von Mises stress in the material, and λ_1 is the lowest buckling load of the structure. Here, a material section is defined to be an individual ground structure member or a section of the skin bordered by the members of the ground structure. Design variables could include both Boolean variables defining whether a member exists in the structure and scalar variables defining thicknesses of existing members. For simplicity, only Boolean variables are used in this study.

The optimization framework is outlined in Figure 1. The inputs of the process are the geometric definitions of the outer mold line (OML) shape and the ground structure, as well as the loading of the wing. To start the process, the OML generator and the ground structure generator are used to produce the OML geometry of the wing and a ground structure filling the OML geometry. The ground structure involves a large number of structural candidates, from which the structural optimizer picks candidates to be included the final, optimized design. Two evolutionary optimizers[a] are used: a genetic algorithm (GA) and an evolutionary structural optimization (ESO) algorithm. During the optimization process, finite element (FE) analysis is used to evaluate the feasibility of individuals in terms of the stress and buckling constraints. The final output is the optimal structural topology and the corresponding structural mass.

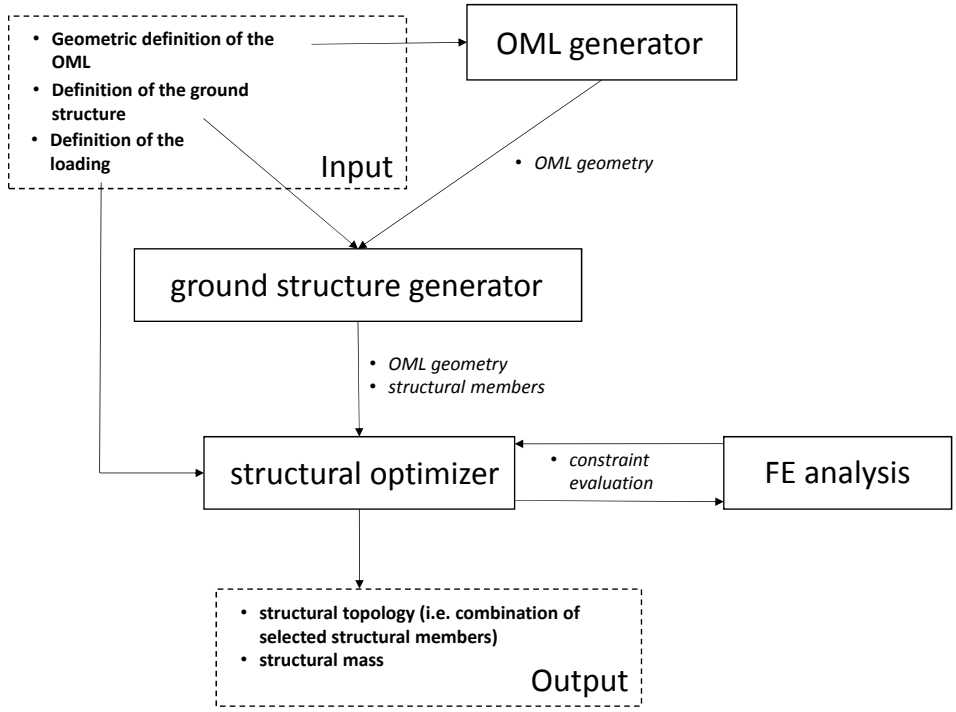

Figure 1: The topology optimization procedure of the internal structures by the ground structure approach.

A. The ground structure and geometry generators

The ground structure consists of a set structural members that are candidates for the final internal structure. As mentioned in the introduction, the ground structure is a finite subset of the structural universe, which is an infinite collection of all possible structural members inside the design space. The density of the ground structure can be varied to meet the given optimization time budget with the available computational resources. The ground structure is always specified inside a given design space. The design space of an aircraft wing internal structure is bounded by the OML of the wing.

In this study, the internal structure of the aircraft wing is a subset of a ground structure consisting of slots, within each of which shell or beam members can be chosen. The member slots are oriented in longitudinal, transverse and two diagonal directions within the wing, and they are perpendicular to the planform surface of the wing. Shell members represent the types of internal structures that extend between the opposite skins of the wing. Traditionally, these structures are called spars and ribs. However, the diagonal ground structure elements are included to expand the search space and the flexibility of the optimization. The beam members are located at the intersections of member slots and the external skin. These members represent stiffeners attached to the skin panels. The beam members are given a cross-section, which is aligned to be

[a]We follow the literature in the way we refer to both GA-type searches and ESO-type heuristics as 'evolutionary', but with the caveat that only the former is truly 'evolutionary' in the sense of mimicking Darwinian evolution (though the latter also has elements of survival guided by the virtual 'environment').

inside the wing, perpendicular to the skin panel. Naturally, a member slot can also be left empty. Figure 2 presents the four member options for a slot, indexed from 0 to 3, where index 0 is an empty slot and index 1 is a full-depth member. The weight of full-depth members is reduced by a lightening hole in the middle of the member. The hole has an elliptical shape, and its dimensions are determined as a fraction c_{oh} of the main dimensions of the member. Using only indices 0 and 1 would define a pure on/off ground structure of full-depth member. However, indices 2 and 3 are included as intermediate choices to place either stiffeners on both skins or on the upper skin only, respectively. A stiffener located only on the lower skin is not included amongst the options, because the positive load factor is always greater (in absolute value) than the negative load factor.

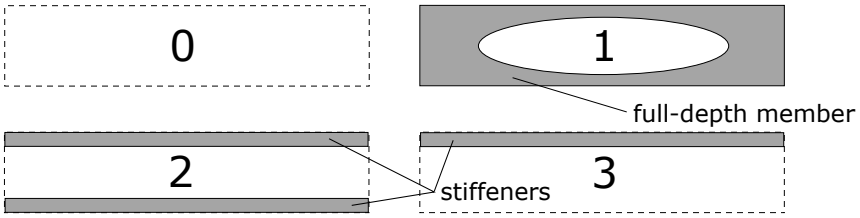

Figure 2: Options for ground structure members.

Both the ground structure and the OML geometry of the wing are generated automatically using parametric geometries. We refer to these modules as ground structure and OML generators, respectively. In our implementation both of these modules use Python scripting in Rhinoceros to generate NURBS (Non-Uniform Rational B-Splines) surfaces. The OML generator uses an open-source collection of Python objects, called AirCONICS (Aircraft Configuration through Integrated Cross-disciplinary Scripting)[b], developed by Sóbester.[27] The ground structure generator uses a newly developed set of Python objects, called AirSTRUCT. The modules are able to define OML shapes and ground structures of both conventional and unconventional wings. Two visualized ground structures and corresponding OML shapes made with these modules are presented in Section III.C.

B. Evolutionary optimization

Two alternative optimization algorithms are used to decide which ground structure members are included in the final structure. These optimization algorithms, i.e. genetic algorithm (GA) and (bi-directional) evolutionary structural optimization ((B)ESO), are presented in the following.

1. GA-based optimization method

GAs are optimization methods that mimic the natural evolution. Solution candidates are encoded as *strings*, in a similar fashion to a DNA molecule containing the genetic representation of a living organism. A set of strings form a population, from which the fittest individuals have the best chance to reproduce to the next generation (cf. natural selection). GAs are gradient-free global search methods that perform well on non-differentiable functions and functions with many local optima.[28] The current optimization problem has a multi-modal landscape, as many different subsets of ground structure members have a similar objective function value. The GA-based optimization method should have the potential of selecting the optimal, or a nearly optimal, subset of ground structure members.

As mentioned in Section II.A, each ground structure slot has three options, indexed from 0 to 3 (a full-depth member, stiffeners on the upper and lower skin or a stiffener on the lower skin only). These indices are considered as elements of a string. The default number of member options is four, but the designer can easily suppress or add options.

In the experiments reported on here we tested two approaches to encoding the elements into a string. In the first approach, called one-dimensional encoding, the elements are organized in a vector form. Starting from the beginning of the vector, first all elements corresponding to longitudinal ground structure slots are encoded on the vector. Then, all elements corresponding to transverse and the diagonal slots, in this order, are added to the vector. Thus, the length of the vector is the same as the total number of slots in the ground

[b]Available at www.aircraftgeometry.codes

structure. The second approach is to use two-dimensional encoding, where the elements are organized into a matrix form based on the physical location of the corresponding ground structure slot in the wing.

The two-dimensional string is more likely to maintain geographical linkage of elements close to each other in the ground structure. Figure 3 illustrates the geographical linkage in a crossover of two individuals encoded on two-dimensional strings. The first parent only has the transverse slots of the ground structure filled with full-depth members, whereas the second parent only the longitudinal slots filled with either full-depth or upper skin stiffeners. The crossover is conducted with a clear diagonal cut. As it can be seen, the offspring has a significant number of features from both different parents.

While the crossover in Figure 3 is an artificial example designed to illustrate the principle behind the operator proposed here, the crossover operators in GAs are randomly defined. Here, the crossover operator of one-dimensional strings is defined to use a cut at two random points of a string (Figure 4a). This crossover is usually termed *two-point crossover*. The two-point crossover has been widely used for one-dimensional strings. The crossover for two-dimensional strings could be done in its simplest form by slicing the string with either horizontal or vertical lines. However, this would lead to a low diversity of crossover operators.[29] A better solution is to use more randomized operators. In this study, grid points are defined in between the elements and a random path is chosen through the grid points. The grid has a total of $(m+1)(n+1)$ points, where m and n are the dimensions of the two-dimensional string. The random path is generated by first picking a random grid point at the domain boundary and then repeatedly moving to another grid point either left, straight or right with respect to the last two points. The process is ended when another boundary is reached (Figure 4b) or the path becomes self-intersecting (Figure 4c). We shall term this operator *random walk* crossover. Two parameters are used to control the development of the path in the random walk crossover. First, p_s is the probability for the path to move to a point straight ahead of the current point. The remaining left and right turns have the same probability of $(1-p_s)/2$. A treshold value N_{min} is used as a minimum number of elements from both parents in the offspring. If the treshold value is not reached a new splicing path is generated. Several combinations of parameters p_s and N_{min} were tested, and reasonable crossover operators with a reasonable level of diversity were obtained using values: $p_s = 0.6$ and $N_{min} = 0.05$.

The design problem is constrained by the allowable von Mises stress and the lowest critical buckling load. These constraints need to be taken into account when defining the GA driven optimization framework. The simplest way of handling constraints in a GA is to penalize the fitness of constraint violating designs to the extent that they are guaranteed not to survive. However, if multiple constraints exist, finding a feasible point might be nearly as difficult as finding the optimum, which may well make this approach impractical. Discarding the infeasible offspring also reduces the diversity of the population, which might lead to premature convergence to a local optimum.

A common alternative is to translate the constrained optimization problem into an unconstrained problem by applying a penalty function. In order to bias the search towards offspring containing a significant amount of genetic material from each parent, the penalty function approach with a constant penalty coefficient is chosen in this study (see Yeniay[30] for a review of penalty function methods in GA-based optimization). Thus, Equation 1 becomes

$$\begin{aligned} \text{minimize} \quad & W_s(x) + r_s \sum_{i=1}^{n} c_{s,i}(x) + r_b c_b(x) \\ \text{w.r.t} \quad & x_i \qquad\qquad i = 1, 2, \ldots, m, \end{aligned} \tag{2}$$

where r_s and r_b are penalty coefficients of violated stress and buckling constraints, respectively. The coefficients are tuned so that the penalty terms have a similar amplitude as the objective term. Variables $c_{s,i}$ and c_b accommodate possible penalties from the stress and buckling constraints, respectively. The stress penalty is determined independently in the n sections of the structure. The variables are defined as

$$c_{s,i} = \begin{cases} \sigma_i^{max} - \sigma^{limit}, & \text{if } \sigma_i^{max} \geq \sigma^{limit} \\ 0, & \text{otherwise} \end{cases} \tag{3}$$

$$c_b = \begin{cases} 1 - \lambda_1, & \text{if } \lambda_1 \leq 1 \\ 0, & \text{otherwise.} \end{cases} \tag{4}$$

In terms of computational implementation, for the GA experiments described in this paper we used

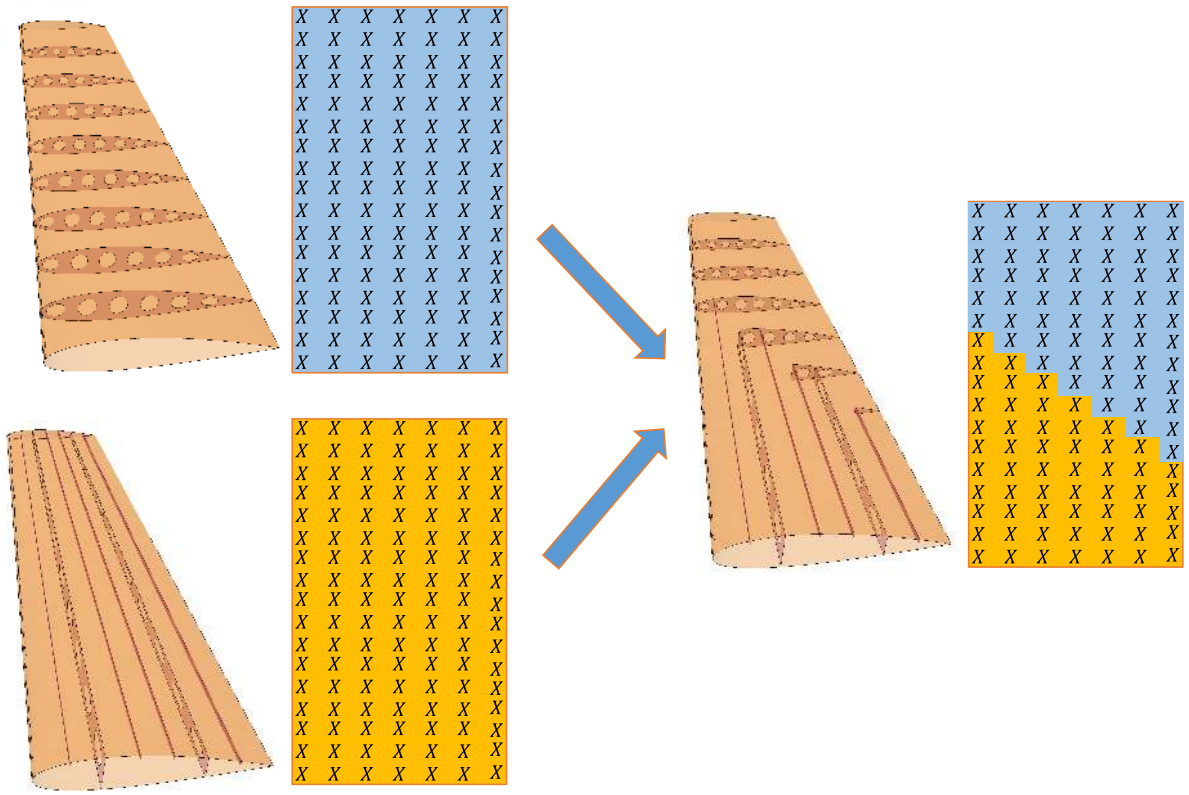

Figure 3: Example of crossover between two-dimensional strings representing wing designs.

Pyevolve,[31] an open source library of evolutionary operators, capable of parallel processing and implementing a set of one- and two-dimensional crossover operators (to which we have added the random walk crossover).

2. (B)ESO-based optimization method

ESO is a structural optimization method, which iteratively removes structural elements with lesser utilization, or importance. The method was first presented by Xie and Stevens.[32] The idea is that after each iteration a sensitivity number α is determined for all elements in the structure based on their utilization. At each iteration elements are rejected if their sensitivity is lower than

$$\alpha_{reject} = RR_j \alpha_{max}, \tag{5}$$

where RR_j is the prevailing rejection rate of the iteration j and α_{max} is the maximum sensitivity number in the structure at the same iteration j. At the start of an ESO process, rejection rate RR_j is given a low value, which is increased when the process proceeds. Iterations are repeated until a predefined stopping criterion is met. The stopping criterion may be, for example, a minimum sensitivity number level for all elements in the structure or a desired volume fraction of the design space.

Before going into the details of ESO, let us define what a rejection of a member means in the current study. As described in Section II.A, four member options are given for each member slot in the ground structure. In terms of the whole wing structure, these options have the following hierarchy: full-depth member (index 1), stiffeners on upper and lower skins (index 2), stiffener on the upper skin (index 3) and an empty slot (index 0). The higher the hierarchy, the more the option is assumed to strengthen the wing. The rejection of a member is defined as moving one step down in the hierarchy.

The determination of the sensitivity number is critical to effective ESO. Sensitivity calculation methods have been developed for stress, displacement, buckling and frequency constraints. As mentioned earlier, this study considers only stress and buckling constraints, so only these sensitivity models are considered. For

(a) One-dimensional splice

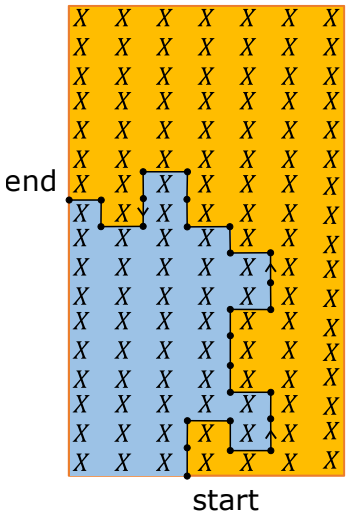

(b) Two-dimensional splice ending at a grid boundary point

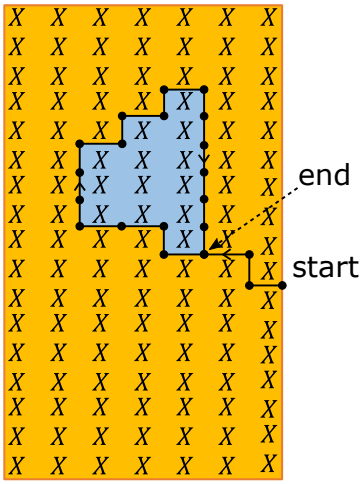

(c) Two-dimensional splice ending at a self-intersecting point

Figure 4: Examples of the crossover of one- and two-dimensional strings, where X represents an element, and colors blue and yellow correspond to genes coming from parents 1 and 2, respectively. One-dimensional strings are spliced using two-point crossover, whereas two-dimensional strings are spliced using the random walk crossover.

others and for a more extensive description of ESO and BESO methods the reader may refer to Refs. 33 and 34. For stress, the sensitivity number α_i of an element i can be simply defined as

$$\alpha_i = \sigma^{vm}_{max}, \tag{6}$$

where σ^{vm}_{max} is the maximum von Mises stress of the element. The sensitivity number for buckling is normally defined as

$$\alpha_i = -\{u^i_1\}^T[\Delta K^i]\{u^i_1\}, \tag{7}$$

where $\{u^i_1\}$ is the eigenvector of the element i in the lowest buckling mode, and $[\Delta K^i]$ is the change in the stiffness matrix of the same element (the derivation of the equation is presented, for example, in the paper by Manickarajah et al.[35]). However, if sensitivity number is used to optimize shell structures, the thickness distribution in the shell must be continuous.[33] Therefore, individual elements cannot be rejected from the structure. This conflicts with the aims of the current optimization study, wherein we are considering wholesale changes in topology.

Because of the sensitivity number limitation, an alternative approach is selected for the evaluation of element sensitivities. At each iteration, the buckling sensitivities of the elements are determined by individually removing elements from the structure and comparing its lowest eigenvalue to the reference structure as

$$\alpha_i = \lambda_i - \lambda_{ref}, \tag{8}$$

where λ_i is the lowest eigenvalue of the structure without element i, and λ_{ref} is the lowest eigenvalue of the reference structure having all the remaining elements. It is to be noted that the approach is computationally more expensive than the classical way of determining the sensitivity numbers for all elements from a single FE analysis.

We also adopt an alternative definition of the rejection rate RR_j. The reason is that, if multiple members are rejected from a certain region of the ground structure in the same iteration, the critical buckling load may suddenly drop under the stopping criterion. Therefore, to have a better control of the number of rejected members, at each iteration N_{rej} members with the smallest sensitivities are rejected.

In ESO, the rejection of an element is irreversible, which might lead the optimization to a local optimum. To overcome this problem, Querin et al.[36] introduced bi-directional ESO (BESO), where rejected elements may be added back to the structure. Two formulations of BESO exist in the literature. The *soft-kill* formulation does not remove a rejected element but changes its elastic modulus to a small value, which reduces its effect to the stiffness matrix of the structure. The other formulation, called *hard-kill*, removes the entire element from the FE mesh. In this study, we explored the use of both ESO and BESO. With BESO, the hard-kill formulation is used in the FE analysis, and the maximum number of recovered elements per iteration is limited to $N_{recovery}$.

C. Constraint evaluation (FE analysis)

The wing structure is required to withstand the applied loads without an occurrence of two classical failure mechanisms: yield and loss of structural stability. From an optimization point of view, these requirements are viewed as constraints. The failure mechanisms are measured as the maximum von Mises stress in a section and the lowest critical buckling load in an eigenvalue based buckling analysis. The purpose of the constraint evaluation is to check whether a design point lays in the feasible region, and, if not, to what extent are how much the constraints violated. The challenge with these constraints is that for a 3-dimensional structure they are highly nonlinear and cannot be expressed analytically. Reasonable accuracy for the constraint evaluation is achieved with finite element (FE) analysis, which is a well established method for numerical analysis of structural mechanics. The von Mises stress distribution is determined by a static analysis, and the lowest critical buckling load using an eigenvalue analysis.

FE analyses are performed in Abaqus using its Python based scripting interface. Pre- and post-processing of the FE analysis are fully automated, because a large number of constraint evaluations are required during the optimization process. The pre-processing script generates an FE mesh of the geometries that were produced by OML and ground structure generators, assigns materials to its sections and sets the loads. The structural members that are included in the FE model are determined by the structural optimizer. The post-processing script fetches the von Mises stress distribution and the lowest critical buckling load, and returns them to the structural optimizer.

The structural members can be either full-depth members or stiffeners. The full-depth members, as well as the skin sections, are modeled as shell elements, whereas the stringers are modeled as beam elements. The full-depth members are meshed with triangular elements. If the diagonal slots are included in the ground structure, the skin sections are meshed using a quad-dominated algorithm (produces both triangular and quad elements). If not, the sections are meshed with quad elements, which is computationally more efficient. The beam elements are located at the root of the stiffener so that they use the same nodes as the shell elements of the skins. The beam elements are assigned a cross-section with an L-shape. All elements are first order elements, so triangular and quad elements have 3 and 4 nodes, respectively. The mesh densities were defined so that full-depth ground structure members have at least 4 element in shortest directions, while the same minimum number for the most critical skin sections at the root is 7 elements. Several mesh densities were tested, and these element numbers yielded a reasonable accuracy while maintaining a feasible computational time.

Two types of loads are applied to the FE model: an air load as a pressure load on the upper and lower skins and an inertial load as a body force on all elements of the model. The air load has an elliptical load distribution along the wing span. The total magnitude of the air load corresponds to the take-off mass m_{to} minus the wing mass under the positive limit load factor $n = 4.5$. The wing mass is included in the model as a body force having an amplitude of ng, where n is the limit load factor and g the gravitational acceleration.

III. Application: Topology optimization of a sUAV wing

In this section we apply the ground structure based topology optimization methods on a design of a small unmanned aerial vehicle (sUAV) wing manufactured from 3D printed nylon. The task is to design internal structures inside the OML that minimize the structural mass of the wing subject to buckling, stress, and manufacturing constraints. The final results are benchmarked against corresponding results obtained by traditional design methods.

A. Description of the design problems

The choice of 3D printing as the manufacturing technique sets two main geometric constraints for the design of the wing: maximum bounding box dimensions and minimum wall thickness. Let us refer to these as manufacturing constraints.

In this study, the material is chosen to be nylon, which is commonly used in additive manufacturing. The material and manufacturing related properties of the material are listed in Table 1[c]. Nylon, as well as other 3D printed materials, are known to have anisotropic material properties depending on the direction in which they are layered. Majewski and Hopkinson[37] experimented with the material properties of Laser Sintered (LS) Nylon-12 rods using a tensile testing, in which the thickness and layering orientation of the rods was varied. The tensile properties of the material were described to be robust to changes in material thickness and building orientation. Based on the experiments the Young's modulus and tensile strength in the weakest direction were estimated to be roughly 80 and 94 per cent, respectively, of the the corresponding properties in the strongest direction. Therefore, and for the sake of simplicity, the material is assumed in this study to have homogeneous mechanical properties.

Ensuring that a wing can be printed as a whole, the aircraft was chosen to have a semispan of 650 mm, which is equal to the maximum bounding box edge length. The geometric definition of the wing is given in Table 2. The wing profile is defined using 4-digit NACA profiles transitioning linearly from the root to the tip. A relatively low aspect ratio was chosen to encourage the development of a variety of internal structures in both directions.

Parameter	Value	Unit
elastic modulus	1700	MPa
Poisson's ratio	0.39	-
yield strength	48	MPa
density	930	kg/m^3
min wall thickness	0.7	mm
max bounding box	650 x 350 x 550	mm

Table 1: Material and manufacturing properties of 3D printed nylon.

Parameter	Value	Unit
semispan	650	mm
aspect ratio	7	-
total wing area	0.241	m^2
taper ratio	0.5	-
sweep angle at leading edge	5.0	deg
dihedral angle	0.5	deg
root profile	NACA2420	-
tip profile	NACA2412	-

Table 2: Geometric definition of the sUAV wing.

The wing is required to withstand the loads without buckling or yielding under positive ($n = 4.5$) and negative ($n = -1.0$) limit load factors (Table 3). To evaluate these constraints, the following loads are applied to the FE model of the wing. First, a pressure load is applied to the upper and lower surfaces of the wing to describe the aerodynamic forces. The pressure corresponds to a maximum take off weight W_{TO} of 2.41 kg assuming that the weight of the wings, which is excluded from the pressure load, is 12 per cent of the maximum take-off weight. The maximum take-off weight was chosen to result in a wing loading that is realistic for a sUAV (10 kg/m^2). The pressure load has an elliptical load distribution along the wing span. Second, inertial loads are applied on the wing weight as body forces with an amplitude ng, where g is the

[c]www.shapeways.com (revisited on 10th March 2016)

gravitational acceleration. The inertial loads act in the opposite direction to the pressure load, and therefore decrease the total loading on the wing.

Parameter	Value	Unit
max take-off weight W_{TO}	2.41	kg
load factor range n	-1.0...4.5	-
wing loading W_{TO}/S	10	kg/m^2
factor of safety λ_s	1.5	-

Table 3: Load properties of the sUAV wing.

As the first step of the design task, the textitlightest manufacturable design was analyzed, in which no internal structures were placed inside the OML and the entire skin was defined to have a thickness equal to the minimum wall thickness. The design clearly has the smallest mass that still fulfills the manufacturing constraints. With the positive limit load factor, the maximum von Mises stress in the structure is 7.48 MPa, which is, by a good margin, less than the yield stress of the material (Table 1). However, the structure buckles when only 44.0 % of the design load is applied (Figure 6a). With the negative limit load factor, the maximum von Mises stress is 1.66 MPa, and the structure buckles at 93.0 % of the design load. The shape of the buckling mode has its greatest values in either the upper or the lower skin near the root depending on the load factor (the positive load factor causes buckling of the upper skin). In both cases the buckling occurs first near the trailing edge where the curvature of the skin is the smallest.

As a conclusion of analysis of the lightest manufacturable design, the structure is not likely to yield under positive or negative limit load factors with any internal structure arrangement. Thus, the stress constraint is not evaluated in the optimization process. In contrast, the buckling constraint under positive load factor is clearly an active constraint for the optimization and needs to be evaluated in the optimization process. Under the negative load factor, the skin alone with only the minimum wall thickness is almost strong enough to resist buckling. When the structure is stiffened to the buckling under the positive load factor, the critical buckling load under the negative load factor is likely to be above the design load. Thus, the buckling constraint evaluation under the negative load factor is excluded from the optimization process to reduces the computational cost of the analysis. To ensure the feasibility of the final design, all excluded constraints are verified after the optimization process.

B. Conventional designs methods

The buckling resistance of a wing structure can be improved by increasing its skin thickness or by adding internal structures, such as spars, ribs and stiffeners, inside the wing. This section presents three conventional design methods, starting from the simplest, to meet the required buckling strength. The results are benchmarks for the topology optimization.

The simplest way to provide the required buckling strength for a sUAV wing is to increase its skin thickness, which was set to the lower manufacturing constraint in the lightest manufacturable design. This approach is simple but obviously will not yield the best structure. Using a skin thickness of 0.956 mm, the normalized critical buckling load under load factor $n = 4.5$ becomes unity and therefore the design is feasible. Since only the skin thickness was varied, the modal shape of the critical buckling mode (c.f. Figure 6b) is almost identical to the lightest manufacturable design. The weight addition with respect to the lightest manufacturable design is 41.4 grams.

In any case, increasing the skin thickness is rather naive way to fulfill the design criteria. A better solution is to stiffen the structure with spars, ribs and stiffeners. In the next design approach, called *traditional design*, two spars are placed at 15 and 65 % of the chord, respectively, and four ribs are evenly distributed in the spanwise direction (Figure 5a). Finally, several FE iterations were performed to find the minimum number of spanwise stiffeners that provide a feasible design. In the critical buckling mode the greatest displacements are near the root of the upper skin, which buckles between the spars and stiffeners (Figure 6c). In comparison to the lightest manufacturable design, the structural weight is increased by 32.7 grams.

The skin thickness in this example is relatively high due to the manufacturing constraint. Thus, the traditional design involving spars and ribs is likely to be over-sized for the purpose. Therefore, only spanwise and chordwise stiffeners are used in the last design approach, called *stiffener design*, to obtain a more efficient

manually designed structure. After several iterations, a design was obtained where the six spanwise stiffeners and two rims of chordwise stiffeners are located near the root of the wing (Figure 5b). The lowest critical buckling mode is plotted in Figure 6d. Since the weight increment to the lightest manufacturable design is only 7.67 grams, the stiffener design is significantly better than the increased skin thickness design or the traditional design.

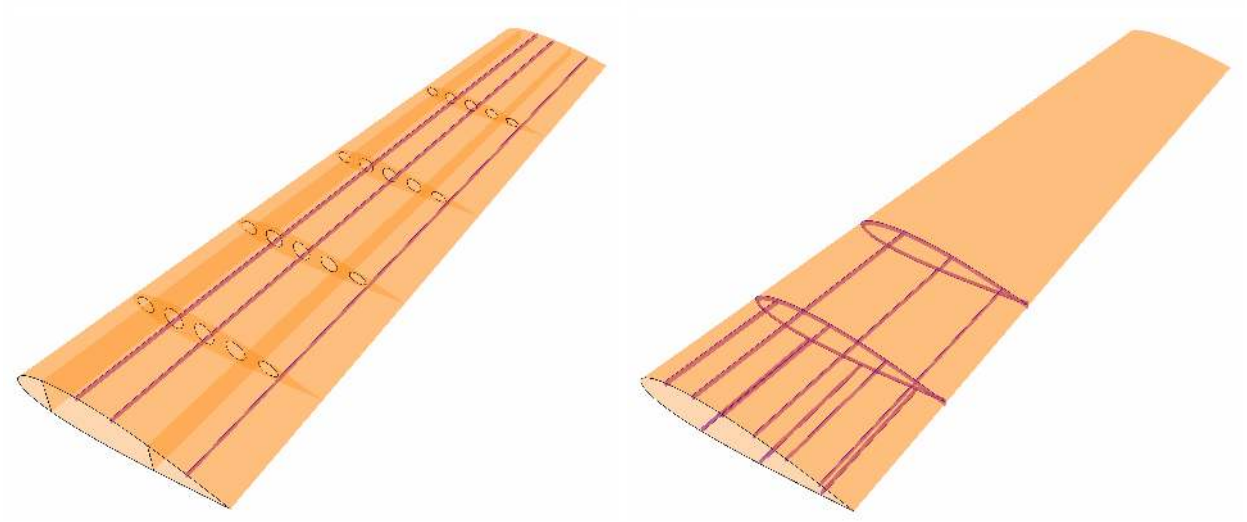

(a) Conventional design with spars, ribs and stiffeners

(b) Conventional design with stiffeners only

Figure 5: Two examples of conventional internal structures. The internal structures have been designed manually using conventional spars, ribs and stiffeners.

C. Ground structures of topology optimization

The ground structures are generated inside the OML of the sUAV wing using the methods described in Section A. However, since the purpose of the internal structures is in this case only to stiffen the upper skin of the wing against buckling, member option 2 (stiffeners on the upper and lower skins) is suppressed. Basically the same stiffening effect for the upper skin is obtained with option 3 (stiffener on the upper skin). Two alternative ground structures are used in the optimization.

The first (GS1) (Figure 7a) is a simple ground structure with 6 longitudinal and 8 transverse member slots. For simplicity, it does not have diagonal members. The total number of member slots is 110. The stiffener members have an L-profile of 4 x 0.8 mm, and a component thickness of 0.7 mm, which is the same as the minimum wall thickness. Lightening holes, with a size fraction $c_{oh} = 0.6$ (cf. Section II.A), are added to the full-depth members to reduce their weight.

GS2 (Figure 7b) incorporates two improvements over GS1. First, the diagonal member slots are added to the ground structure, while keeping the number of longitudinal and transverse members the same as in GS1. The reason for diagonal members is that, as mentioned in the literature review, some studies have indicated that their addition may improve the efficiency of the final structure. Second, the transverse slots are placed in a geometric series, where each transverse slot gap is 1.1 times the previous one (starting from the root). This modification shifts more member slots to the root of the wing, where more internal structure is typically needed. The total number of member slots in GS2 is 173.

D. Results and discussion

The aforementioned topology optimization methods are deployed on the two grounds structures, GS1 and GS2, defined in Section III.C. The content of this section is as follows. First, we use GS1 to tune essential parameters of both GA- and (B)ESO-based optimizations. Results of these parameters studies are presented in Sections III.D.1 and III.D.2, respectively. In addition, these sections present the variation of the critical buckling load during the two optimization methods. Second, optimization runs with GS2 are performed by

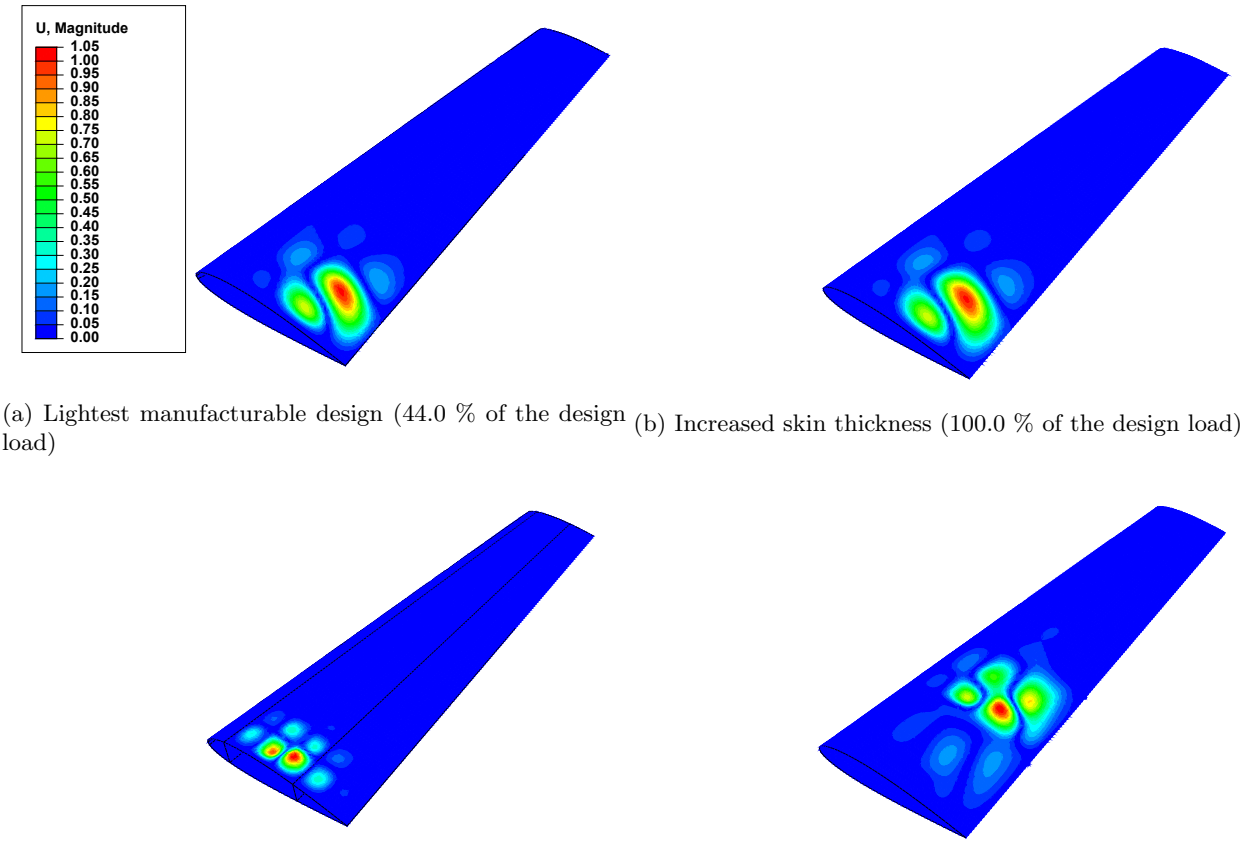

(a) Lightest manufacturable design (44.0 % of the design load)

(b) Increased skin thickness (100.0 % of the design load)

(c) Traditional design (107.4 % of the design load)

(d) Stiffener design (106.5 % of the design load)

Figure 6: Modal shapes of the first critical buckling load for wings designed with traditional methods.

exploiting the gathered parameter information from GS1. Finally, the two optimization methods, as well as the two ground structures, are compared to each others and benchmarked against the conventional designs methods (Section III.D.3).

1. GA-based optimization results

The varied parameters for the GA-based optimization are the encoding type (one- or two-dimensional encoding) and the population size. Other GA parameters are kept constant; the crossover and mutation rates are 0.9 and 0.02, respectively, and no elitism is used. Further, tournament selection with a pool size of four is used, and the mutation operator is set to swap the locations of two randomly selected elements of the string. Since GAs are stochastic, multiple optimization runs are to be executed to obtain statistical evidence on whether a parameter value has a better performance than another.

Optimization runs using one- and two-dimensional encodings were both repeated three times. Based on the convergence histories plotted in Figure 8a, the one-dimensional encoding seems to yield slightly faster convergence and better final designs than the two-dimensional encoding. This result is against the hypothesis that two-dimensional encoding, due to better geographical linkage of elements, would provide better results in design problems with a two-dimensional architecture. However, we must note that due to the small sample size this comparison is not statistically significant. Here, the population size N has a value of 150.

Next, the population size N is varied. The determination of a reasonable population size is crucial in a GA-based optimization, especially if function evaluations are computationally expensive. Too small a population may cause a loss of diversity among the individuals, which may lead to a premature convergence to a local optimum. On the other hand, an over-sized population may make the search inefficient. The convergence histories of the optimization with four different population sizes are presented in Figure 8b. The

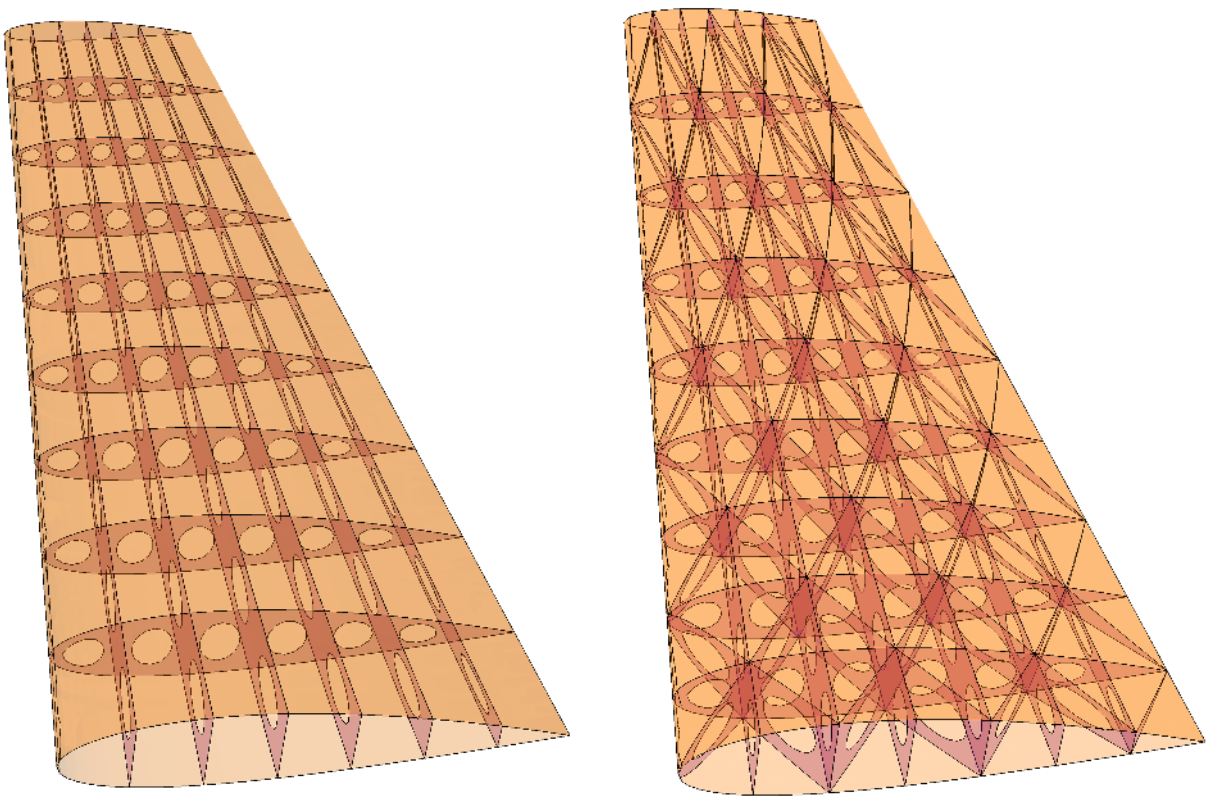

(a) Ground structure 1

(b) Ground structure 2

Figure 7: Two examples of conventional internal structures. The internal structures have been designed manually using conventional spars, ribs and stiffeners.

abscissa is the number of function evaluations. As we can see, the optimized mass seems to be independent of the population size within the tested range. Therefore, even the smallest population size ($N = 75$), with the lowest computational cost, may be adequate to reach the global, or nearly global, optimum. However, more optimization runs are again needed for statistically significant conclusions on the adequate population size. The one-dimensional encoding is used in all of these optimization runs.

A penalty has been applied on the objective function of individuals violating the buckling constraint. The stress constraint is not evaluated (see reasoning in Section III.A). The optimization method was tested with penalty coefficients $r_b = 0.1, 1, 10$. The aim was to find a value for the penalty coefficient so that the objective and penalty terms in Equation 2 have roughly the same amplitude. Out of the three tested values, penalty coefficient $r_b = 1$ was found to be the best for the purpose. To illustrate the effect of the penalty function, Figure 9 presents the constraint and objective function values of all individuals during optimization run 1 (infeasible individuals are marked with grey in Figure 9b). As we can see, in the zeroth generation, in which all individuals are randomly generated, most of the individuals are infeasible. However, during the next generations the penalty function biases the search towards feasible designs; this is seen as a rapid increase in the number of feasible individuals per generation. The number of feasible individuals reaches its maximum at the fourth generation, after which it starts to decrease. We assume this behavior to be caused by the selective pressure driving the individuals towards ground structure subsets with smaller number of members. When fewer members are included in the individuals of a generation, removal of a critical member by the genetic operators becomes more likely.

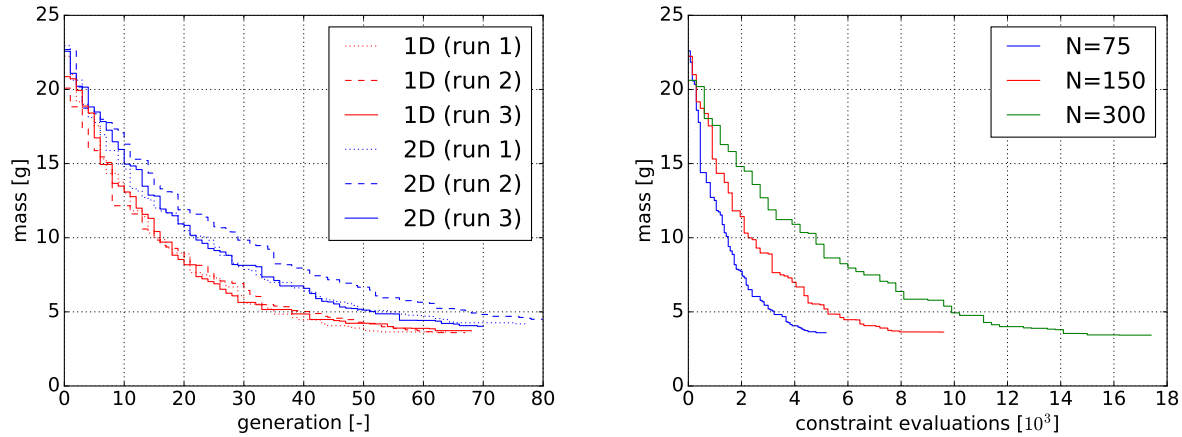

(a) (b)

Figure 8: Comparisons of one- and two-dimensional encodings (a) and the effect of the population size (b) in the results of the GA-based optimization method.

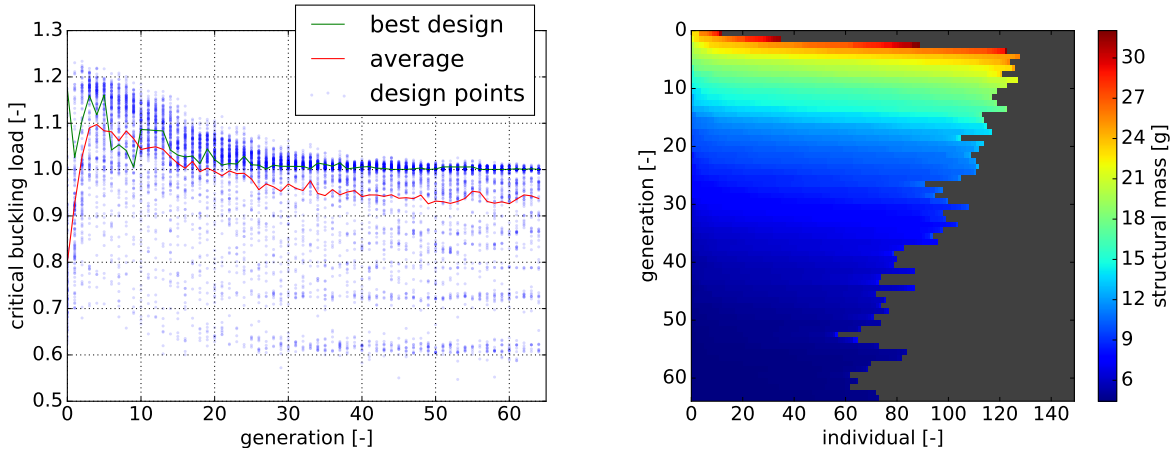

(a) (b)

Figure 9: Representation of all individuals in a GA-based optimization run. The constraint function (a) is the critical buckling load, whereas the objective function (b) is the structural mass.

2. (B)ESO-based optimization results

Three optimization parameters are varied in the evaluation of the (B)ESO-based optimization method. The first is whether members are allowed to be recovered back to the structure (BESO) or not (ESO), and the second is the number of rejected members per iteration, N_{rej}. With BESO, the third parameter was added to define the maximum number of recovered members per iteration, N_{rec}. Table 4 summarizes the five optimization runs. Since (B)ESO is a deterministic optimization method, runs were not repeated. The number of rejected members is defined to decrease as a function of the iteration number. The reason is that the sensitivities of the members are tested individually without actually knowing the combined sensitivities of a set of members. This is not critical in the beginning of the process, where several members can be removed at the same iteration without significantly decreasing the critical buckling load. However, towards the end of the process the structure becomes more sensitive and the risk of rejecting a set of members with a significant combined sensitivity increases.

Figure 10 presents the evolution of the internal structure mass (a) and critical buckling load (b) as a

function of the iteration number. Since the same ground structure (GS1) is used in all optimization runs, they all start from the same structural mass and critical buckling load. During the first iterations, the critical buckling load actually increases, which seems to run contrary to intuition. We believe that the reason is in the definition of the member option hierarchy. In the beginning of the rejection process members are changed from full-depth members to stiffeners on the upper skin, which at some parts of the structure seem to provide better resistance against buckling.

Optimization runs 1 and 2 were executed first to compare the performances of ESO and BESO-based optimization methods with a fairly coarse rejection plan (see Table 4). As it can be seen from Figure 10b, the critical buckling load decreases rapidly at around iterations 15-18, an indication that too many members have been rejected from the same region during an iteration. Optimization run 2 uses the BESO definition with unlimited number of member recoveries. As a consequence, the rapid decrease in the critical buckling load triggers an oscillation phenomenon, where several members are moved back and forth between two regions of the wing on consecutive iterations. Eventually, the oscillation causes the termination of the process when the critical buckling load becomes less than unity. To avoid the oscillation, a maximum number of member recoveries per iteration, N_{rec} is introduced. As we can see in the figure, optimization run 3, executed with $N_{rec} = 2$, has a more stable behavior than optimization run 2. Meanwhile, the critical buckling load of optimization run 1, where no recoveries are made, increases steadily form 1.03 to 1.15. In a similar fashion to in the beginning of the optimization, several full-depth members are changed to stiffeners on the upper skin during these iterations. However, the behavior is not fully understood. With the coarse rejection plan, optimization runs with ESO- (run1) and BESO-based (run3) methods yield similar results.

Next, ESO- (run 4) and BESO-based (run 5) optimizations were performed with a finer rejection plan. This time no rapid decrease was observed during the optimization. For most of the optimization process, the BESO-based optimization has slightly greater critical buckling load than the ESO-based optimization. In contrast to the coarse rejection plan, this time the BESO-based optimization method yields 3.55 grams lighter design than the ESO-based optimization method.

run ID	(B)ESO	N_{rej}	N_{rec}
1	ESO	iter. 0-10: 10	N/A
		iter. 10-20: 5	
		iter. 20-: 3	
2	BESO	iter. 0-10: 10	unlimited
		iter. 10-20: 5	
		iter. 20-: 3	
3	BESO	iter. 0-10: 10	2
		iter. 10-20: 5	
		iter. 20-: 3	
4	ESO	iter. 0-15: 6	N/A
		iter. 15-30: 3	
		iter. 30-50: 2	
		iter. 50-: 1	
5	BESO	iter. 0-15: 6	1
		iter. 15-30: 3	
		iter. 30-50: 2	
		iter. 50-: 1	

Table 4: Parameter combinations of the executed (B)ESO-based optimization runs.

3. Comparison of the methods

The design task of the sUAV wing internal structure has been performed using conventional design and topology optimization methods. We shall next compare the results of GA- and (B)ESO-based topology optimization methods, and evaluate their performance against conventional design methods, presented in

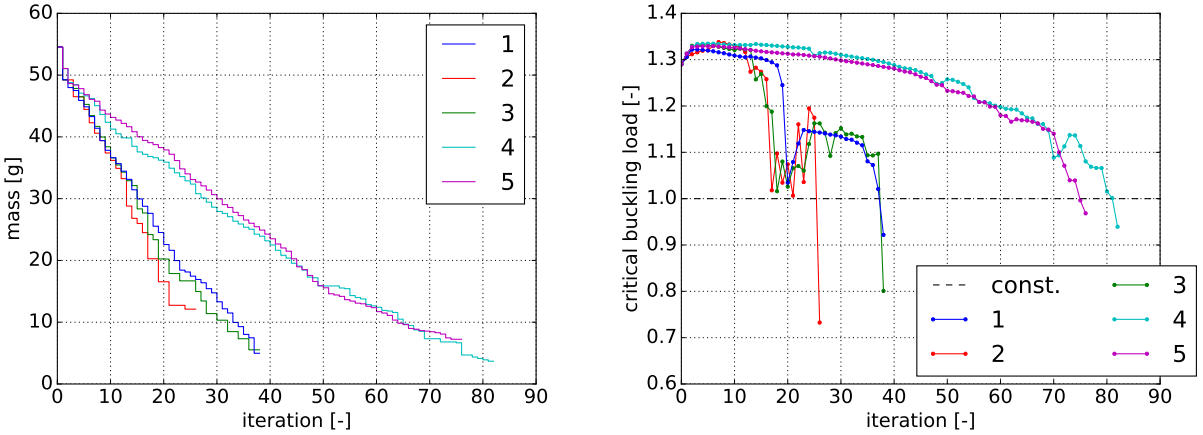

(a) (b)

Figure 10: Variation of the internal structure mass (a) and the critical buckling load during (B)ESO-based optimization runs on GS1.

Section III.B. Representative optimization runs with GS1 are selected for the comparison, and, in addition, two new runs are performed with the computationally more expensive GS2. The methods and corresponding values for the internal structure mass are listed in Table 5. All final design are feasible, i.e. they do not violate any constraints specified in Section III.A.

Method	pop. size N	encoding	rej. & rec.	optimized mass [g]
incr. skin thickness	N/A	N/A	N/A	41.4
traditional design	N/A	N/A	N/A	32.7
stiffener design	N/A	N/A	N/A	7.67
GS1 (GA)	300	1D	N/A	3.43
GS1 (BESO)	N/A	N/A	Plan 1	3.68
GS2 (GA)	300	2D	N/A	3.24
GS2 (ESO)	N/A	N/A	Plan 2	2.73

Table 5: Comparison of the design methods. For (B)ESO-based methods, Plan 1 is N_{rej} = iter. 0-15: 6; iter. 15-30: 3; iter. 30-50: 2; iter. 50-: 1 and $N_{rec} = 1$, whereas Plan 2 is N_{rej} = iter. 0-25: 6; iter. 25-50: 3; iter. 50-80: 2; iter. 80-: 1 and and $N_{rec} = N/A$ (ESO-based optimization).

The convergence history of the internal structure mass is plotted in Figure 11 with corresponding values obtained from the conventional design methods. The internal structure mass at the first generation for GA-based methods is the mass of the best design out of $N = 300$ randomized individuals, where the corresponding mass for the (B)ESO-based method equals to the ground structure filled with full-depth members. Therefore, the mass at the first iteration of the (B)ESO-based method is higher than the corresponding mass at the first generation of the GA-based method. In addition, the structural mass in the beginning for GS2 is higher than the corresponding mass for GS1, because more member slots are included in GS2. All the final designs are in the range of 2.73 to 3.68 grams, where the ESO-based optimization initiated from GS2 yields the lightest design. Representative intermediate designs and the final, optimized design are visualized in Figure 12 for all four optimization runs. The designs have similar features with each others. All desings have several continuous lines of longitudinal stiffeners (on the upper skin) starting from the root of the wing around the mid-chord. In addition, they all have a two to five full-depth members close to the trailing edge. These full-depth members provide also buckling resistance for the lower skin, which is prone for a snap-through buckling. Despite the fact the designs have similar features, they are clearly not identical. Thus, the current optimization problem has a very multi-modal landscape where local optima are found in abundance.

Considering that the number of different subsets of members drawn from GS2 is $3^{173} \approx 3.48 \times 10^{82}$, finding the global optimum is nearly impossible. However, finding a good local optimum is often sufficient for practical design tasks.

The first objective of the paper was to explore alternative structural arrangements for the presented sUAV wing design brief. The obtained designs are clearly different, and better in terms of the structural mass, compared to/than the traditional spar-rib arrangements (see Figure 5a). However, because of the minimum wall thickness specified in the design brief, the role of the internal structure is unusual. While the over-sized skin alone carries all the stresses in the wing, the purpose of the internal structure is only to prevent the skin from buckling. Therefore, we cannot directly extrapolate the obtained results to aircraft wings in general.

The second objective was to benchmark the topology optimization methods against conventional design methods. The best conventional design, i.e. the stiffener design (Figure 5b), is outperformed by both GA- and (B)ESO-based optimization methods. The obtained design from the ESO-based optimization method with GS2 is 64 % lighter than the stiffener design.

The presented topology optimization methods could be used for automated design optimization of a number of conventional and unconventional wings. The skin and the internal structure can be defined to be made of any isotropic material.

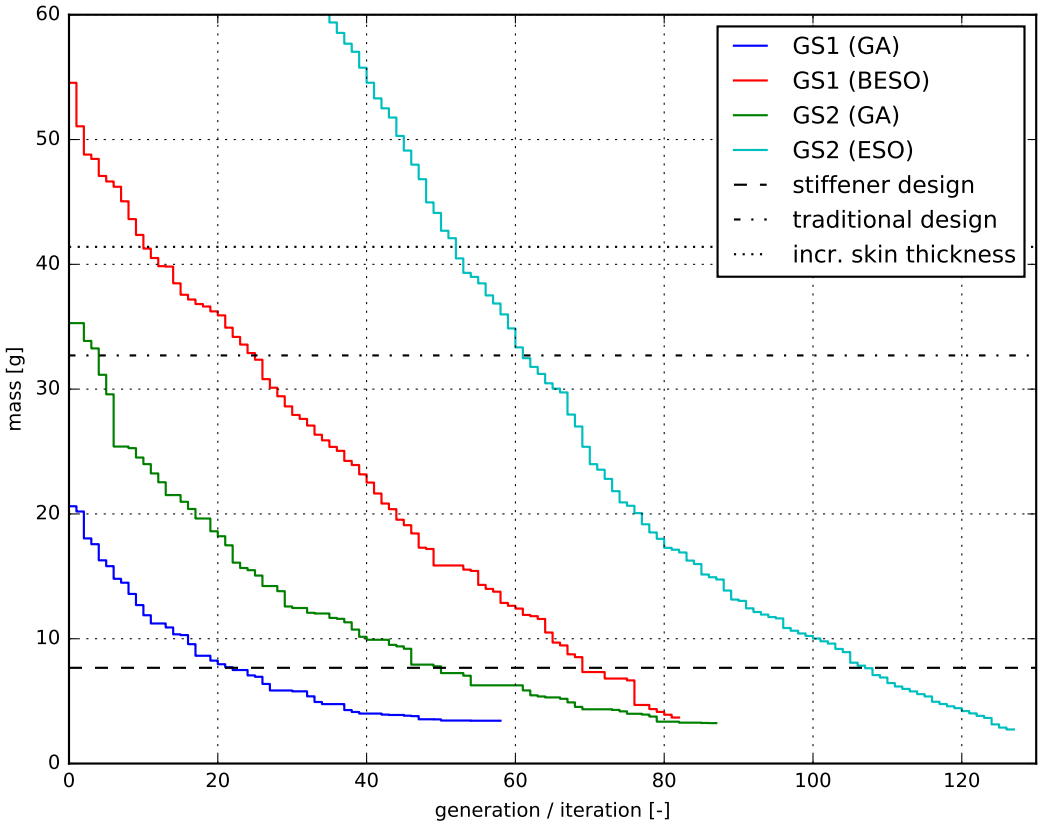

Figure 11: Comparison of the convergence histories of the representative BA- and (B)ESO-based optimization methods. The methods are benchmarked against three conventional design methods.

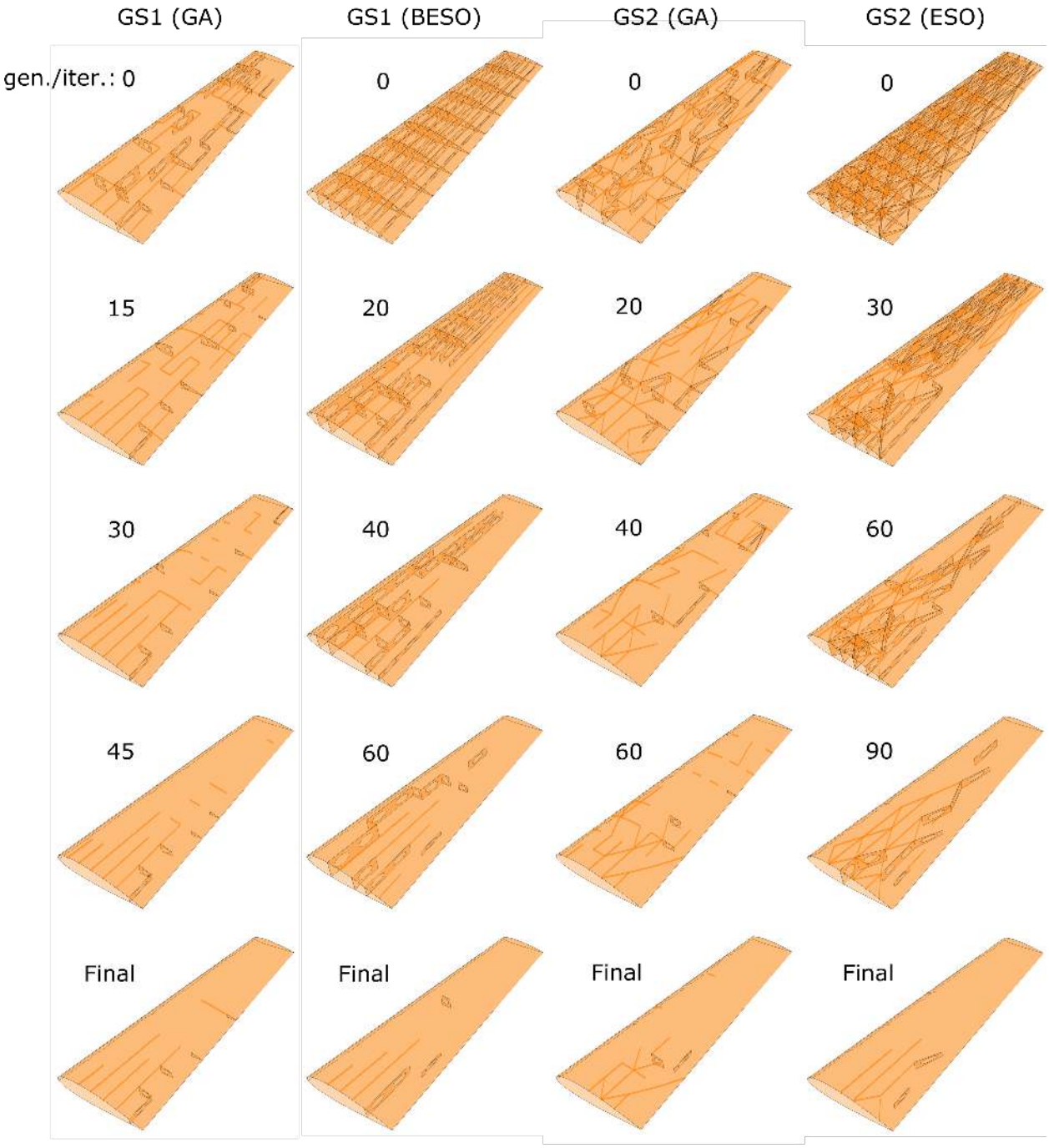

Figure 12: Evolution of the internal structure using the GA- and (B)ESO-based optimization methods on GS1 and GS2.

IV. Conclusion

This paper presents GA- and (B)ESO-based optimization methods for the topology optimization of a sUAV wing structure. The resulting designs do not have the familiar spar-rib arrangement typical of conventional aircraft wing structures, which raises interesting questions in terms of wing structural design

in general. We have presented a small study here, limited to sUAV wings built via additive manufacturing; clearly, more extensive studies are required to gauge the potential of the methodology described here in the wider context of aircraft wing design.

Acknowledgments

The authors are grateful to the Finnish Cultural Foundation, and the Engineering and Physical Sciences Research Council (UK) for sponsoring the work.

References

[1]Jakab, P. L., "Wood to metal: The structural origins of the modern airplane," *Journal of Aircraft*, Vol. 36, No. 6, 1999, pp. 914–918.

[2]Balabanov, V. and Haftka, R. T., "Topology optimization of transport wing internal structure," *Journal of Aircraft*, Vol. 33, No. 1, 1996, pp. 232–233.

[3]Wang, W., Guo, S., and Yang, W., "Simultaneous partial topology and size optimization of a wing structure using ant colony and gradient based methods," *Engineering Optimization*, Vol. 43, No. 4, 2011, pp. 433–446.

[4]Yang, W., Yue, Z., Li, L., and Wang, P., "Aircraft wing structural design optimization based on automated finite element modelling and ground structure approach," *Engineering Optimization*, , No. 1, 2016, pp. 94–114.

[5]Lencus, A., Querin, O. M., Steven, G. P., and Xie, Y. M., "Aircraft wing design automation with ESO and GESO," *International journal of vehicle design*, Vol. 28, No. 4, 2002, pp. 356–369.

[6]Bendsøe, M. P. and Kikuchi, N., "Generating optimal topologies in structural design using a homogenization method," *Computer methods in applied mechanics and engineering*, Vol. 71, No. 2, 1988, pp. 197–224.

[7]Eves, J., Toropov, V. V., Thompson, H. M., Gaskell, P. H., Doherty, J. J., and Harris, J., "Topology optimization of aircraft with non-conventional configurations," *Proceedings of the 8th World Congress on Structural and Multidisciplinary Optimization*, 2009.

[8]James, K. A. and Martins, J. R. R. A., "An isoparametric approach to level set topology optimization using a body-fitted finite-element mesh," *Computers & Structures*, Vol. 90, 2012, pp. 97–106.

[9]Dunning, P. D., Stanford, B. K., and Kim, H. A., "Aerostructural Level Set Topology Optimization for a Common Research Model Wing," *AIAA SciTech Conference*, 2014, pp. 1–21.

[10]Oktay, E., Akay, H. U., and Sehitoglu, O. T., "Three-dimensional structural topology optimization of aerial vehicles under aerodynamic loads," *Computers & Fluids*, Vol. 92, 2014, pp. 225–232.

[11]Stanford, B. K. and Dunning, P. D., "Optimal topology of aircraft rib and spar structures under aeroelastic loads," *Journal of Aircraft*, Vol. 52, No. 4, 2014, pp. 1298–1311.

[12]Locatelli, D., Mulani, S. B., and Kapania, R. K., "Wing-Box Weight Optimization Using Curvilinear Spars and Ribs (SpaRibs)," *Journal of Aircraft*, Vol. 48, No. 5, 2011, pp. 1671–1684.

[13]Jutte, C. V., Stanford, B. K., Wieseman, C. D., and Moore, J. B., "Aeroelastic tailoring of the NASA common research model via novel material and structural configurations," *AIAA SciTech Conference*, 2014, pp. 13–17.

[14]Kelly, L., Keane, A. J., Sobester, A., and Toal, D. J. J., "Topology Optimisation: Increasing the Speed and Reliability of Design," *15th AIAA/ISSMO Multidisciplinary Analysis and Optimization Conference, AIAA Aviation. American Institute of Aeronautics and Astronautics*, 2014.

[15]Kobayashi, M. H., LeBon, A., Pedro, H. T. C., Kolonay, R. M., and Reich, G. W., "On a cellular division model for multidisciplinary optimization," *51st AIAA/ASME/ASCE/AHS/ASC Structures, Structural Dynamics, and Materials Conference*, 2010, p. 2989.

[16]Hansen, L. U. and Horst, P., "Multilevel optimization in aircraft structural design evaluation," *Computers & structures*, Vol. 86, No. 1, 2008, pp. 104–118.

[17]Gen, M. and Cheng, R., *Genetic algorithms and engineering optimization*, Vol. 7, John Wiley & Sons, 2000.

[18]Bui, T. N. and Moon, B. R., "On multi-dimensional encoding/crossover," *Proceedings of the 6th International Conference on Genetic Algorithms*, Morgan Kaufmann Publishers Inc., 1995, pp. 49–56.

[19]Cohoon, J. P. and Paris, W. D., "Genetic placement," *IEEE Transactions on Computer-Aided Design of Integrated Circuits and Systems*, Vol. 6, No. 6, 1987, pp. 956–964.

[20]Chou, T.-Y., Liu, T.-K., Lee, C.-N., and Jeng, C.-R., "Method of inequality-based multiobjective genetic algorithm for domestic daily aircraft routing," *IEEE Transactions on Systems, Man and Cybernetics, Part A: Systems and Humans*, Vol. 38, No. 2, 2008, pp. 299–308.

[21]Ono, I., Yamamura, M., and Kobayashi, S., "A genetic algorithm for job-shop scheduling problems using job-based order crossover," *Proceedings of IEEE International Conference on Evolutionary Computation*, IEEE, 1996, pp. 547–552.

[22]Kim, J., Hwang, I., Kim, Y.-H., and Moon, B.-R., "Genetic approaches for graph partitioning: a survey," *Proceedings of the 13th annual Conference on Genetic and Evolutionary Computation*, 2011, pp. 473–480.

[23]Giger, M. and Ermanni, P., "Evolutionary truss topology optimization using a graph-based parameterization concept," *Structural and Multidisciplinary Optimization*, Vol. 32, No. 4, 2006, pp. 313–326.

[24]Neves, M. M., Rodrigues, H., and Guedes, J. M., "Generalized topology design of structures with a buckling load criterion," *Structural Optimization*, Vol. 10, No. 2, 1995, pp. 71–78.

[25]Pedersen, N. L., "Maximization of eigenvalues using topology optimization," *Structural and Multidisciplinary Optimization*, Vol. 20, No. 1, 2000, pp. 2–11.

[26]Browne, P. A., Budd, C., Gould, N. I. M., Kim, H. A., and Scott, J. A., "A fast method for binary programming using first-order derivatives, with application to topology optimization with buckling constraints," *International Journal for Numerical Methods in Engineering*, Vol. 92, No. 12, 2012, pp. 1026–1043.

[27]Sóbester, A., "Four Suggestions for Better Parametric Geometries," *10th AIAA Multidisciplinary Design Optimization Conference*, American Institute of Aeronautics and Astronautics, 2014, pp. 1–10.

[28]Whitley, D., "A genetic algorithm tutorial," *Statistics and Computing*, Vol. 4, No. 2, 1994, pp. 65–85.

[29]Kahng, A. B. and Moon, B. R., "Toward More Powerful Recombinations," *Proceedings of the 6th International Conference on Genetic Algorithms*, 1995, pp. 96–103.

[30]Yeniay, O., "Penalty function methods for constrained optimization with genetic algorithms," *Mathematical and Computational Applications*, Vol. 10, No. 1, 2005, pp. 45–56.

[31]Perone, C. S., "Pyevolve: a Python open-source framework for genetic algorithms," *ACM SIGEVOlution*, Vol. 4, No. 1, 2009, pp. 12–20.

[32]Xie, Y. M. and Steven, G. P., "Shape and layout optimization via an evolutionary procedure," *Proceedings of the International Conference on Computational Engineering Science*, 1992.

[33]Munk, D. J., Vio, G. A., and Steven, G. P., "Topology and shape optimization methods using evolutionary algorithms: a review," *Structural and Multidisciplinary Optimization*, Vol. 52, No. 3, 2015, pp. 613–631.

[34]Huang, X. and Xie, M., *Evolutionary topology optimization of continuum structures: methods and applications*, John Wiley & Sons, 2010.

[35]Manickarajah, D., Xie, Y. M., and Steven, G. P., "Optimisation of columns and frames against buckling," *Computers & Structures*, Vol. 75, No. 1, 2000, pp. 45–54.

[36]Querin, O., Steven, G., and Xie, Y., "Evolutionary structural optimisation (ESO) using a bidirectional algorithm," *Engineering Computations*, Vol. 15, No. 8, 1998, pp. 1031–1048.

[37]Majewski, C. and Hopkinson, N., "Effect of section thickness and build orientation on tensile properties and material characteristics of laser sintered nylon-12 parts," *Rapid Prototyping Journal*, Vol. 17, No. 3, 2011, pp. 176–180.